


RESEARCH

Open Access



ImmunoPET imaging of amyloid-beta in a rat model of Alzheimer's disease with a bispecific, brain-penetrating fusion protein

Gillian Bonvicini^{1,2}, Stina Syvänen¹, Ken G. Andersson², Merja Haaparanta-Solin^{3,4}, Francisco López-Picón^{3,4} and Dag Sehlin^{1*} 

Abstract

Background: Hijacking the transferrin receptor (TfR) is an effective strategy to transport amyloid-beta (A β) immuno-positron emission tomography (immunoPET) ligands across the blood–brain barrier (BBB). Such ligands are more sensitive and specific than small-molecule ligands at detecting A β pathology in mouse models of Alzheimer's disease (AD). This study aimed to determine if this strategy would be as sensitive in rats and to assess how TfR affinity affects BBB transport of bispecific immunoPET radioligands.

Methods: Two affinity variants of the rat TfR antibody, OX26, were chemically conjugated to a F(ab')₂ fragment of the anti-A β antibody, bapineuzumab (Bapi), to generate two bispecific fusion proteins: OX26₅-F(ab')₂-Bapi and OX26₇₆-F(ab')₂-Bapi. Pharmacokinetic analyses were performed 4 h and 70 h post-injection of radioiodinated fusion proteins in wild-type (WT) rats. [¹²⁴I]-OX26₅-F(ab')₂-Bapi was administered to TgF344-AD and WT rats for in vivo PET imaging. Ex vivo distribution of injected [¹²⁴I]-OX26₅-F(ab')₂-Bapi and A β pathology were assessed.

Results: More [¹²⁵I]-OX26₅-F(ab')₂-Bapi was taken up into the brain 4 h post-administration than [¹²⁴I]-OX26₇₆-F(ab')₂-Bapi. [¹²⁴I]-OX26₅-F(ab')₂-Bapi PET visualized A β pathology with significantly higher signals in the TgF344-AD rats than in the WT littermates without A β pathology. The PET signals significantly correlated with A β levels in AD animals.

Conclusion: Affinity to TfR affects how efficiently a TfR-targeting bispecific fusion protein will cross the BBB, such that the higher-affinity bispecific fusion protein crossed the BBB more efficiently. Furthermore, bispecific immunoPET imaging of brain A β pathology using TfR-mediated transport provides good imaging contrast between TgF344-AD and WT rats, suggesting that this immunoPET strategy has the potential to be translated to higher species.

Keywords: ImmunoPET, Transferrin receptor, Alzheimer's disease, Amyloid-beta

Background

Positron emission tomography (PET) is a useful diagnostic tool for neurodegenerative diseases to visualize and quantify aspects of pathology inside the brain in vivo.

For example, visualization of amyloid-beta (A β) plaques in the brains of Alzheimer's disease (AD) patients with [¹¹C]Pittsburgh Compound B ([¹¹C]PiB) or other fluorine-18 (¹⁸F)-labelled analogues increases the diagnostic confidence of AD [1]. However, these small-molecule tracers do not bind to soluble A β aggregates that are assumed to be the toxic species underlying early AD progression [2, 3] or to diffuse A β plaques such as those found in AD patients with the Arctic APP mutation [4].

*Correspondence: dag.sehlin@pubcare.uu.se

¹ Department of Public Health and Caring Sciences, Uppsala University, 751 85 Uppsala, Sweden
Full list of author information is available at the end of the article



© The Author(s) 2022. **Open Access** This article is licensed under a Creative Commons Attribution 4.0 International License, which permits use, sharing, adaptation, distribution and reproduction in any medium or format, as long as you give appropriate credit to the original author(s) and the source, provide a link to the Creative Commons licence, and indicate if changes were made. The images or other third party material in this article are included in the article's Creative Commons licence, unless indicated otherwise in a credit line to the material. If material is not included in the article's Creative Commons licence and your intended use is not permitted by statutory regulation or exceeds the permitted use, you will need to obtain permission directly from the copyright holder. To view a copy of this licence, visit <http://creativecommons.org/licenses/by/4.0/>. The Creative Commons Public Domain Dedication waiver (<http://creativecommons.org/publicdomain/zero/1.0/>) applies to the data made available in this article, unless otherwise stated in a credit line to the data.

Small-molecule tracers also perform poorly in discriminating between different proteins with similar fibrillary structures (e.g., A β vs alpha-synuclein, a protein which aggregates in Parkinson's disease) [5].

Antibody-based tracers are highly specific to their targets, and were increasingly used for peripheral PET in the oncology field during the last decade [6, 7]. However, one of the main reasons that hinder the use of immunoPET radioligands for central nervous system (CNS) targets is their limited blood–brain barrier (BBB) passage. Only less than 0.05% of the injected antibody dose passes into the brain 2 h after injection, making it difficult to achieve adequate signal-to-noise ratios for in vivo imaging [8–11].

Antibodies can be engineered to utilize endogenous active transport systems at the BBB to enhance brain uptake, such as transferrin receptor (TfR)-mediated transcytosis [12–14]. Targeting the TfR is an effective strategy for increasing brain delivery of therapeutic antibodies and peptides in mice [10, 15–19], rats [20–23], non-human primates [24–26], and human subjects in some clinical trials [27]. This strategy has also proven successful for developing bispecific antibody-based radioligands for A β PET in AD mouse models [7, 9–11, 28–33].

The affinity of bispecific antibodies to TfR influences their BBB-crossing efficacy, and there is an optimal TfR affinity window at therapeutic doses [16, 18, 22, 24, 34–37]. Antibodies with too high affinity are not released on the abluminal side of brain endothelial cells, while antibodies with too low affinity bind to TfR insufficiently for transcytosis and remain in the blood [16, 18, 22, 24]. This relationship is potentially dose-related. At tracer doses, increasing the affinity directly correlates with higher brain uptake [16].

Bispecific antibody-based radioligands targeting both TfR and A β have been shown to detect A β pathology and discriminate between AD and WT mice at an earlier disease stage than [^{11}C]PiB [28, 31, 32]. Moreover, a bispecific antibody-based radioligand is more sensitive than [^{11}C]PiB at detecting reductions in A β levels in two AD mouse models after treatment with an A β -reducing BACE-1 inhibitor [7]. These studies indicate that the bispecific immunoPET radioligands can image more subtle changes in A β pathology than small-molecule tracers.

Given this background, the primary aim of this study was to evaluate if immunoPET imaging of A β aggregates is equally sensitive in rats as in mice. The second aim was to assess the role of TfR affinity in transport of immunoPET radioligands across the BBB, using two bispecific fusion proteins with different TfR-affinity, OX26₅-F(ab')₂-Bapi and OX26₇₆-F(ab')₂-Bapi.

Materials and methods

Recombinant protein expression and purification

Two variants of the mouse anti-rat TfR (rTfR) antibody, OX26, were produced: OX26₅ and OX26₇₆ [22, 38]. OX26₅ is the WT OX26 antibody and OX26₇₆ has a single alanine mutation in the complementarity determining region 1 on the heavy chain variable region. Both OX26 variants were expressed as mouse IgG2c molecules. The extracellular domain of rTfR (L101 to F761) was also produced with flag and 10xHis tags attached to the C-terminus.

Expression vectors pcDNA3.4 were synthesized by GeneArt Elements (Invitrogen, Carlsbad, CA) and were transfected into the Expi293 Expression System following the manufacturer's instructions (Life Technologies, Carlsbad, CA). Plasmid DNA (100 μg total; 1:1 ratio of heavy to light chain for antibodies) and ExpiFectamine 293 reagent in Opti-MEM[®] I medium were added to the Expi293F cells. Cells were incubated at 37 °C, 120 RPM, with 70% humidity and 8% CO₂ for 20 h before ExpiFectamine 293 Transfection enhancer 1 and 2 were added. Four days later, cell supernatant was harvested for purification.

OX26 variants were purified on a HiTrap Protein G column (Cytiva, Uppsala, Sweden) with an ÄKTA Purifier system (Cytiva) and eluted with an increasing gradient of 0.7% acetic acid (HAc). rTfR was purified on a HisTrap Excel immobilized metal ion affinity chromatography column (Cytiva) with a binding buffer containing 20 mM Tris and 200 mM NaCl and eluted in the binding buffer with 500 mM imidazole. Following elution, all three proteins underwent buffer exchange to phosphate buffered saline (PBS) on a HiPrep 26/10 desalting column (Cytiva).

Biacore analysis of the OX26 affinity to rTfR

With the Biacore 8 K (Cytiva), anti-mouse IgG from the Mouse Antibody Capture Kit, type 2 (Cytiva) was immobilized on flow cells 1 and 2 of a CM5 chip (Cytiva) following kit instructions. Ten micrograms of OX26₅, OX26₇₆, or a commercial control OX26 (LS-C43741, LSBio, Seattle, WA) were captured on flow cell 2. A 1-min regeneration step with 10 nM glycine-HCl (pH 1.7) on flow cell 1 succeeded the capture step to ensure no antibody was captured on the reference flow cell. A single cycle kinetics assay with 5 concentration steps from 3.2 to 2000 nM of rTfR for 2 min each was run over both flow cells, followed by 1 h of dissociation. All dilutions were done in HBS-EP+running buffer (0.01 M HEPES, 0.15 M NaCl, 3 mM EDTA and 0.05% v/v Surfactant P20, Cytiva) supplemented with 0.1% w/v bovine serum albumin (BSA). Data were analysed with Biacore Insight Evaluation 3.0.12.15655 (Cytiva) and was fitted with a 1:1 binding model.

F(ab')₂ fragmentation of bapineuzumab (Bapi)

Bapineuzumab (Bapi; Absolute Antibody, Oxford, UK), a humanized monoclonal antibody binding A β based on the murine antibody 3D6 and former clinical therapeutic candidate [39], was enzymatically cleaved into F(ab')₂ fragments (F(ab')₂-Bapi) with the cysteine protease IdeS in FragIT columns (Genovis AB, Lund, Sweden). IdeS produces a homogenous preparation of F(ab')₂ fragments by cleaving human IgG at a specific site below the hinge region. F(ab')₂ fragments were purified from Fc fragments and uncleaved antibodies with CaptureSelect Fc (multi-species) Affinity Resin (ThermoFisher Scientific, Stockholm, Sweden). The F(ab')₂ purity was assessed with SDS-PAGE under non-reducing conditions.

Chemical conjugation and purification of bispecific fusion proteins

Trans-cyclooctene (TCO)-functionalized OX26₅ or OX26₇₆ was chemically conjugated to tetrazine-functionalized F(ab')₂-Bapi via an inverse-electron-demand Diels–Alder (IEDDA) reaction to produce two bispecific fusion proteins: OX26₅-F(ab')₂-Bapi and OX26₇₆-F(ab')₂-Bapi.

To prepare for chemical conjugation, OX26₅ or OX26₇₆ (2 mg/ml) was incubated with a 20-fold molar excess of axial TCO-NHS (Conju-Probe, LLC, San Diego, CA) and F(ab')₂-Bapi (4 mg/ml) with a 7-fold molar excess of Tetrazine-PEG5-NHS (Sigma-Aldrich, Stockholm, Sweden) in PBS with 30 mM carbonate buffer (pH 9.6) for 2.5 h, with shaking in darkness at room temperature (RT). After incubation, the buffer was exchanged to PBS with Zeba spin desalting columns 7 K MWCO to remove any free TCO-NHS or Tetrazine-PEG5-NHS. Modified OX26 affinity variants were incubated with 1.5-fold molar excess of modified F(ab')₂-Bapi, with shaking in darkness at RT. After 30 min, a 200-fold molar excess of methyltetrazine-amine HCl salt (Click Chemistry Tools, Scottsdale, AZ) was added to stop any unreacted TCOs from conjugating to unreacted tetrazine on F(ab')₂-Bapi and forming large multi-antibody complexes. Reactions were incubated for another 30 min in darkness before free tetrazine was removed with Zeba spin desalting columns 7k MWCO. Proteins were separated via gel filtration chromatography on a HiLoad[®] 26/600 Superdex[®] 200 prep grade column (Cytiva) using an ÄKTA Purifier system. Components of each fraction were assessed with SDS-PAGE. Approximately 2 μ g of protein was mixed with LDL Sample Buffer (ThermoFisher Scientific), loaded onto a NuPAGE 3%–8% Tris-Acetate gel (ThermoFisher Scientific) and run at 150 V for 1 h with NuPAGE Tris-Acetate SDS Running Buffer (ThermoFisher Scientific). The gel was washed in water, fixed

Table 1 Radiochemical reaction yield and specific activity of radioligands

Radioligand	Reaction yield (%)	Molar activity (MBq/nmol)
[¹²⁴ I]-OX26 ₅ F(ab') ₂ Bapi	57.0 \pm 6.9	60.0 \pm 24.2
[¹²⁵ I]-OX26 ₅ F(ab') ₂ Bapi	21.6 \pm 11.2	26.5 \pm 26.6
[¹²⁴ I]-OX26 ₇₆ F(ab') ₂ Bapi	58.5 \pm 3.1	209.1 \pm 5.9

in 50% methanol and 7% HAc solution, and stained with GelCode Blue Stain Reagent (ThermoFisher Scientific).

Radiochemistry

OX26₅-F(ab')₂-Bapi and OX26₇₆-F(ab')₂-Bapi were radiolabelled with iodine-124 (¹²⁴I) or iodine-125 (¹²⁵I) by the direct iodination Chloramine-T method (Table 1) [40].

For ¹²⁴I-labelling, 31.5 \pm 9.9 MBq of ¹²⁴I stock solution (Advanced Centre Oncology Macerata, Montecosaro, Italy) was pre-incubated with 33.3% v/v sodium iodine (NaI, 50 μ M) for 15 min, and then neutralized with 0.5% HAc and 11.1% v/v 10xPBS. Then, 92.9 \pm 57.2 μ g of OX26₅-F(ab')₂-Bapi or 37.0 \pm 0 μ g of OX26₇₆-F(ab')₂-Bapi and Chloramine-T (final concentration 0.1 mg/ml, Sigma-Aldrich) were added to the pre-incubated ¹²⁴I solution. The reaction was quenched after 120 s by adding sodium metabisulfite (final concentration 0.2 mg/ml, Sigma-Aldrich).

For ¹²⁵I-labelling, either 60 μ g of OX26₅-F(ab')₂-Bapi or 23.4 μ g of OX26₅-F(ab')₂-Bapi modified with Bolton-Hunter reagent, as described previously [28], was mixed with 11.1 \pm 1.1 MBq of ¹²⁵I stock solution (PerkinElmer Inc., Waltham, MA), Chloramine-T (final concentration 40 μ g/ml) and PBS to a final volume of 110 μ l. After incubating 90 s at room temperature, the reaction was stopped with sodium metabisulfite (final concentration 74 μ g/ml).

Radiolabelled products were diluted to 500 μ l with PBS, purified of free iodine with a disposable NAP-5 size exclusion column (Cytiva) and eluted in 1 ml of PBS. Radiolabelling was performed no more than 2 h prior to each in vivo study.

Quality control of radiolabelled bispecific fusion proteins

Sandwich ELISA was performed to determine the concentrations of bispecific fusion proteins after radiolabelling using plates coated with 2 nM anti-mouse-IgG (#AI-2000, Vector Laboratories Inc., Newark, CA). Indirect ELISA was performed to assess the potential effects of conjugation and radiolabelling on the binding of OX26₅-F(ab')₂-Bapi or OX26₇₆-F(ab')₂-Bapi to rTfR and

Table 2 Number of rats (male/female), injected radioactivity, and dose for the pharmacokinetic (PK) and the PET studies

Radioligand	PK study		PET study		Injected radioactivity (MBq)	Injected dose (mg/kg)
	WT		WT	TgF344-AD		
	4 h	70 h	3 days	3 days		
[¹²⁴ I]-OX26 ₅ F(ab') ₂ Bapi	—	—	2/2	4/1	13.0 ± 6.1	0.12 ± 0.08
[¹²⁵ I]-OX26 ₅ F(ab') ₂ Bapi	2/0	2/0	—	—	0.9 ± 0.1	0.04 ± 0.02
[¹²⁴ I]-OX26 ₇₆ F(ab') ₂ Bapi	2/0	3/0	—	—	6.1 ± 1.3	0.04 ± 0.01

A β , using plates coated with 13.3 nM of rTfR or 50 nM of A β (Innovagen, Lund, Sweden), respectively.

ELISA assays were performed in 96-well half-area plates (Corning Inc., New York, NY). Plates were coated with respective proteins diluted in PBS overnight at 4 °C and then blocked with 1% BSA in PBS for 1 h. All further dilutions were made in ELISA incubation buffer (PBS with 0.1% BSA, 0.05% Tween and 0.15% Kathon). Control antibodies (OX26₅, OX26₇₆ and Bapi) and the bispecific fusion proteins before and after radiolabelling were serially diluted from 50 nM to 3.2 pM, incubated overnight at 4 °C, washed and then detected with horseradish peroxidase (HRP)-coupled goat anti-mouse IgG-F(ab')₂ (1:2000, #115-035-006, Jackson ImmunoResearch Laboratories, West Grove, PA) or goat anti-human IgG-F(ab')₂ (1:2000, #109-036-006, Jackson ImmunoResearch Laboratories). Signals were developed with K blue aqueous TMB substrate (Neogen Corp., Lexington, KY), halted with 1 M H₂SO₄ and read with a spectrophotometer at 450 nm. The EC₅₀ values were calculated from agonist concentration vs response curves with variable slope (four parameters) where the bottom was constrained to 0 in GraphPad Prism.

Animals

Animals were housed with *ad libitum* access to food and water in an approved animal facility at Uppsala University with controlled temperature and humidity. All procedures in this study were approved by the Uppsala County Animal Ethics board (5.8.18–20401/2020) following the rules and regulations of the Swedish Animal Welfare Agency and in compliance with the European Communities Council Directive of 22 September 2010 (2010/63/EU).

WT Fischer 344 rats (Janvier Labs, Le Genest-Saint Isle, France) were used in the pharmacokinetic studies, and TgF344-AD rats and WT littermates for PET scans. The TgF344-AD rats express human APP with the Swedish mutation (*A β PP KM670/671NL*) and human PSEN1 with exon 9 deletion (*PS1- Δ E9*). They begin displaying age-dependent A β plaque pathology at 6 months [41, 42]

and do not show any sex differences in A β pathology load [41, 43].

Pharmacokinetic study

Three-month-old male WT rats were lightly sedated with isoflurane (Isoflurane Baxter®, Baxter Medical AB, Kista, Sweden) and injected in the tail vein with either [¹²⁵I]-OX26₅-F(ab')₂-Bapi or [¹²⁴I]-OX26₇₆-F(ab')₂-Bapi (Table 2). The rats were anaesthetized with isoflurane 4 h or 70 h post-administration and a terminal blood sample was taken from the heart. The rats were then euthanized by transcardial perfusion with 130 ml of 0.9% NaCl in 8 min to clear the brain and organs of blood. The brain was isolated and dissected into olfactory bulbs, right hemisphere, left cortex, left midbrain and left cerebellum. Brain samples were immediately frozen on dry ice, except for left cortices used for capillary depletion. Lung, heart, liver, pancreas, spleen, kidney, femoral bone, femoral bone marrow, and skull were isolated and a urine sample was collected. Radioactivity from samples was measured with a γ -counter (2480 Wizard™, PerkinElmer Inc.). Concentrations of the bispecific fusion proteins were expressed as standardized uptake values (SUV) to account for variation in weight between animals.

Blood pharmacokinetics

Blood samples (8 μ l) were obtained from the tail vein at 1 h, 4 h, 24 h, and 48 h post-administration. Terminal blood was collected and plasma was separated from the blood cell pellet by centrifugation. Radioactivity was measured with a γ -counter to calculate blood concentration and the percent of free antibody in plasma.

Whole blood half-life was estimated with a non-linear regression two-phase decay model. The plateau was constrained to zero. Y₀ was fixed to 14.3 based on the assumption that 100% of the injected dose enters the blood immediately after injection and the average rat blood volume is 7% of their body weight [44]. The fusion protein exposure, quantified as area under the curve (AUC), was calculated from the SUV blood curves.

Capillary depletion

Capillary depletion was performed on perfused left cortices of rats euthanized 4 h post-injection of [^{125}I] I-OX26₅-F(ab')₂-Bapi or [^{124}I] I-OX26₇₆-F(ab')₂-Bapi. Immediately after transcardial perfusion, cortices were isolated, weighed and homogenized in 2 ml cold physiological buffer (10 mM HEPES, 141 mM NaCl, 4 mM KCl, 2.8 mM CaCl₂, 1 mM MgSO₄, 1 mM NaH₂PO₄, 10 mM D-glucose, pH 7.4) with 8 strokes in an ice-cold Dounce homogeniser. Then 4 ml of 30% Ficoll 400 (Sigma-Aldrich) was added, followed by an additional 2 strokes. The homogenate was centrifuged at 5200 g for 20 min at 4 °C resulting in two fractions: a capillary-enriched pellet and a parenchymal supernatant. Measured radioactivity for each fraction was normalized to the total activity of the homogenate.

PET/computed tomography (CT) imaging

Fourteen-month-old male and female TgF344-AD rats and WT littermates were lightly sedated and injected with [^{124}I] I-OX26₅-F(ab')₂-Bapi in the tail vein (Table 2). The day before injection, animals were given water containing 0.5% NaI to reduce ^{124}I -uptake in the thyroid. After injection, the concentration of NaI was reduced to 0.2% until scanning.

Three days post-injection, rats underwent PET and CT scans. The animals were anesthetized with 5% sevoflurane in 50% medical oxygen and 50% air, and placed on the gantry of a nanoScan[®] PET/MRI 3T system (Mediso Medical Imaging Systems, Budapest, Hungary) in a prone position for a 60–120-min PET scan (Field of view = 9.8 cm). A 5-min CT scan was taken with a nanoScan[®] SPECT/CT system (Mediso Medical Imaging Systems) which is compatible with PET/magnetic resonance image (MRI) and allows for correct image co-registration.

PET data were reconstructed using a Tera-TomoTM 3D algorithm (Mediso Medical Imaging Systems) with 4 iterations and 6 subsets. CT data were reconstructed using Filter Back Projection. Further PET and CT image processing was performed with Amide 1.0.4 [45]. CT and PET scans were manually aligned to a T2-weighted MRI-based rat brain atlas [46]. The following regions of interest were outlined in the MRI: caudate putamen, hippocampi, parietal cortex, occipital cortex, cerebellum and olfactory bulbs. PET data were quantified as mean radioactivity concentrations during the scan expressed as SUV.

Ex vivo analysis of TgF344-AD rats

Immediately after the CT scan, animals were euthanized and dissected as described above, except that brains were dissected into olfactory bulbs, right hemisphere, left cortex (left front half of the cortex), left hippocampus and left cerebellum. Brain samples were immediately frozen

and the radioactivity in the collected tissues, blood and urine samples was measured with a γ -counter. Bispecific fusion protein concentrations were expressed as SUV_{ex vivo} to account for weight variations between animals.

Ex vivo autoradiography

Frozen hemispheres from PET/CT-scanned rats were cryosectioned (CM1850, Leica Biosystems, Nussloch, Germany) into 20- μm sagittal sections. Two sections from each animal were immediately exposed to a phosphor imaging plate (MS, MultiSensitive, PerkinElmer Inc.) for 7 days. The plates were scanned in a Typhoon phosphor imager (Cytiva) at 600 dots per inch. The resulting digital images were converted to a false colour scale (Royal) in ImageJ.

A β immunofluorescence

Sagittal brain slices were fixed in 4% paraformaldehyde and washed in PBS. Antigen retrieval was performed by boiling sections in 25 mM citrate buffer (pH 7.3) for 2 min and leaving them to cool to RT for 40 min. The sections were treated with 70% formic acid (FA) for 10 min, rinsed in milliQ water, washed in PBS and permeabilized in 0.4% Triton in PBS for 5 min. Primary antibody was added to the sections and incubated overnight at 4 °C with slow shaking. The next day, sections were washed in PBS. Secondary antibody was added and incubated for 1 h with shaking at RT, followed by three washes, before mounting with Vectashield Hard Set Mounting medium with DAPI (BioNordika, Solna, Sweden). Fluorescence images were acquired with a Zeiss Observer Z1 microscope (Carl Zeiss Imaging GmbH, Jena, Germany) and processed using ZEN software.

A β ₄₂ immunofluorescence was performed on sagittal brain slices from PET animals. The primary antibody was rabbit anti-human A β ₄₂ (#700,254, Invitrogen) diluted to 1 $\mu\text{g}/\text{ml}$ in 0.1% Tween-20 in PBS. The secondary antibody was Alexa Fluor 488 goat anti-rabbit IgG (1:500 in PBS, #A11008, Invitrogen).

Overall A β immunofluorescence was performed on sagittal brain slices from 15-month-old TgF344-AD and WT rats. Sections were also blocked with Mouse on Mouse (M.O.M.) immunodetection kit (Vector Laboratories) according to kit instructions before permeabilization. The primary antibody was mAb3D6 (murine version of Bapi [47]) diluted to 4 $\mu\text{g}/\text{ml}$ in M.O.M. diluent. The secondary antibody was Alexa Fluor 488 goat-anti-mouse IgG (1:500 in PBS, #A11029, Invitrogen).

Biochemical A β analysis

Brain A β aggregate concentrations in rats that underwent PET scanning were measured with sandwich ELISA as previously described [28]. Briefly, isolated cortex,

hippocampus, and cerebellum were homogenized separately with 4×10 s spins at 5500 rpm in a Precellys® Evolution (Bertin Instruments, Montigny-le-Bretonneux, France) at a 1:5 weight-to-volume ratio in Tris-buffered saline (TBS) with Complete Protease Inhibitor Cocktail Tablets (Roche Diagnostics International AG, Rotkreuz, Switzerland). Samples were centrifuged at 16,000 *g* at 4 °C for 1 h. Supernatants were collected carefully. Pellets were homogenized in 70% FA at a weight-to-volume ratio of 1:5 and centrifuged at 16,000 *g* at 4 °C for 1 h. Again, supernatants were collected.

The concentration of soluble A β aggregates from each brain region was measured by coating a 96-well half-area plate with 145 ng/well of mAb3D6 overnight and blocking with 1% BSA in PBS for 1 h. A β protofibrils (BioArctic) were used as standard. TBS brain extracts were diluted 1:200 and incubated overnight at 4 °C, then detected with biotinylated 3D6 (0.5 μ g/ml) and streptavidin-HRP (1:3000, Mabtech AB, Nacka Strand, Sweden). Signals were developed with K blue aqueous TMB substrate, stopped with 1 M H₂SO₄ and read with a spectrophotometer at 450 nm. In GraphPad Prism 9.1.0, a sigmoidal, 4PL (X is concentration) standard curve was plotted for the interpolation of sample concentrations. All dilutions were made in ELISA incubation buffer.

For total A β ₄₀ and A β ₄₂ concentrations, 96-well half-area plates were coated with 100 ng of polyclonal rabbit anti-human A β ₄₀ (custom production from Agrisera, Vännäs, Sweden) or monoclonal rabbit anti-human A β ₄₂ (#700,254, Invitrogen), respectively. The next day, plates were blocked with 1% BSA in PBS for 1 h. A β ₄₀ (Innovagen) and A β ₄₂ (Innovagen) were used as standards respectively. FA brain extracts were neutralized with 2 M Tris, diluted 1:10,000 and incubated overnight at 4 °C. The procedure continued as described above for the soluble A β aggregate ELISA.

Statistical analyses

Statistical analyses were performed in GraphPad Prism 9.1.0 (GraphPad Software, Inc., San Diego, CA). Results are reported as mean \pm standard deviation. Statistical assessment was carried out by two-tailed *t*-test, one-way ANOVA with Tukey's multiple comparisons test or two-way ANOVA with Šidák's multiple comparisons test. Linear correlation was expressed by Pearson's correlation coefficient.

Results

The K_D of OX26₅ was 4.1 nM and the K_D of OX26₇₆ was 78.4 nM (Fig. 1a), which were consistent with literature [22]. The K_D of the OX26₅ variant was also similar to that of the commercial control, OX26_{LSBio}. Immunofluorescent staining with mAb3D6, the murine version of Bapi, illustrated that this antibody can bind to the A β pathology in TgF344-AD rats but not in WT tissues (Additional file 1: Fig. S1). Therefore, Bapi was a suitable anti-A β antibody for use in the bispecific fusion proteins. OX26₅ or OX26₇₆ was chemically conjugated to F(ab')₂-Bapi to produce two bispecific fusion proteins: OX26₅-F(ab')₂-Bapi and OX26₇₆-F(ab')₂-Bapi (Fig. 1b). The final bispecific fusion protein products contained OX26₅ or OX26₇₆ conjugated to 1–3 F(ab')₂-Bapi, as identified by SDS-PAGE analysis (Fig. 1c, d). Compared to OX26₅, OX26₅-F(ab')₂-Bapi retained its binding to rTfR before and after ¹²⁵I-labelling (Fig. 1e; Table 3). Conversely, OX26₇₆-F(ab')₂-Bapi lost most of its binding to rTfR compared with OX26₇₆. The EC50 of OX26₇₆-F(ab')₂-Bapi, both before and after ¹²⁴I-labelling, was unmeasurable in the given ELISA assay. Both bispecific fusion proteins retained their binding to A β before and after radiolabelling compared to the full Bapi IgG (Fig. 1f; Table 3).

[¹²⁵I]-OX26₅-F(ab')₂-Bapi had higher brain uptake than [¹²⁴I]-OX26₇₆-F(ab')₂-Bapi in WT rats

Four hours post-injection, the concentration of [¹²⁵I] I-OX26₅-F(ab')₂-Bapi in WT rats was 1.3- to 9-fold higher than the concentration of [¹²⁴I] I-OX26₇₆-F(ab')₂-Bapi in the different brain regions measured ($P < 0.01$, Fig. 2a). Capillary depletion 4 h post-injection determined that the majority of the bispecific fusion protein was distributed to the parenchyma (Fig. 2b), with a slightly higher parenchymal portion for [¹²⁴I] I-OX26₇₆-F(ab')₂-Bapi ($P = 0.03$). The whole blood exposure, measured as the AUC, was similar between the bispecific fusion proteins (Fig. 2c), although [¹²⁵I] I-OX26₅-F(ab')₂-Bapi had faster elimination than [¹²⁴I] I-OX26₇₆-F(ab')₂-Bapi in the fast distribution phase (Table 4). The brain-to-blood ratio for [¹²⁵I] I-OX26₅-F(ab')₂-Bapi was significantly higher 70 h post-injection compared with 4 h post-injection ($P = 0.024$) while there was no difference between the two time points for [¹²⁴I] I-OX26₇₆-F(ab')₂-Bapi ($P = 0.999$; Fig. 2d). The brain-to-blood ratio 70 h post-administration was also significantly higher for

(See figure on next page.)

Fig. 1 Generation of bispecific fusion proteins with OX26 affinity variants. **a** Biacore analysis of affinity to rTfR for OX26₅, OX26₇₆ and commercial OX26_{LSBio}. **b** Schematic of the IEDDA reaction to generate OX26-F(ab')₂-Bapi bispecific fusion proteins. **c, d** SDS-PAGE analysis of OX26₅-F(ab')₂-Bapi (**c**) and OX26₇₆-F(ab')₂-Bapi (**d**). Lanes 1, molecular weight ladder; 2, parental OX26 IgG; 3, F(ab')₂-Bapi; 4–5, preparative SEC fractions for the final pool of bispecific fusion protein. **e, f** ELISA analysis of OX26₅-F(ab')₂-Bapi and OX26₇₆-F(ab')₂-Bapi before and after ¹²⁵I-labelling binding to rTfR (**e**) and A β (**f**). RU, response unit; OD, optical density

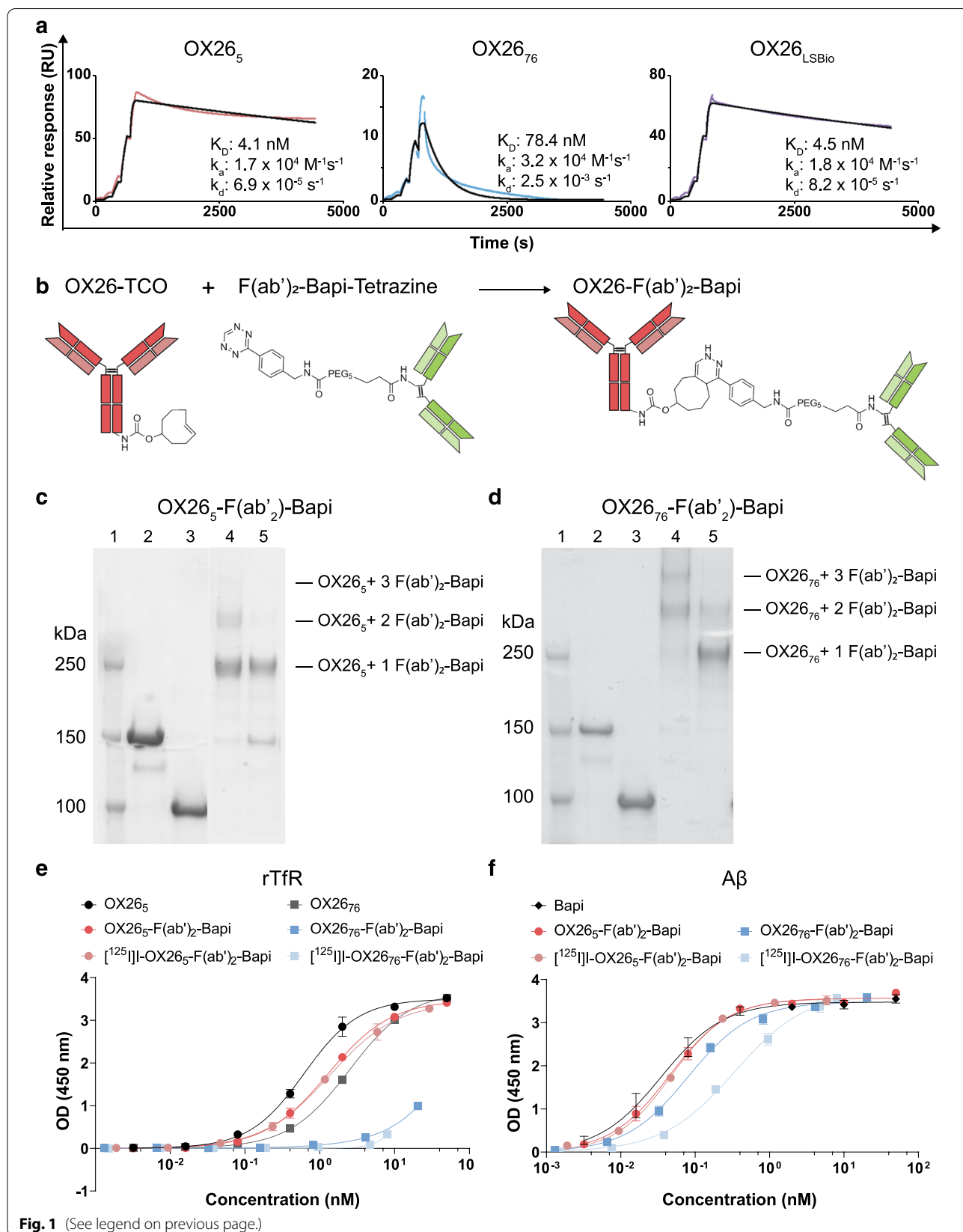


Table 3 EC50 of antibody binding to rTfR or A β in direct ELISA

ELISA target	OX26 ₅	OX26 ₇₆	Bapi	OX26 ₅ -F(ab') ₂ -Bapi		OX26 ₇₆ -F(ab') ₂ -Bapi	
				Unlabelled	[¹²⁵ I]-labelled	Unlabelled	[¹²⁵ I]-labelled
rTfR	0.62	2.54	–	1.28	1.36	Undetectable	Undetectable
A β	–	–	0.03	0.05	0.05	0.08	0.34

[¹²⁵I]-OX26₅-F(ab')₂-Bapi compared to [¹²⁴I]-OX26₇₆-F(ab')₂-Bapi ($P=0.004$), indicating that [¹²⁵I]-OX26₅-F(ab')₂-Bapi entered the brain to a higher extent. The percent in plasma, indicative of the amount of free ligand in the blood, was significantly higher for [¹²⁴I]-OX26₇₆-F(ab')₂-Bapi compared to [¹²⁵I]-OX26₅-F(ab')₂-Bapi at 4 h post-administration ($P=0.018$, Fig. 2e). The peripheral biodistribution was similar for both fusion proteins at 4 h and 70 h post-administration. There was significantly more [¹²⁵I]-OX26₅-F(ab')₂-Bapi than [¹²⁴I]-OX26₇₆-F(ab')₂-Bapi in the spleen at both time points (3.5-fold, $P=0.0002$ at 4 h and 2-fold, $P<0.0001$ at 70 h post-injection) and in the bone marrow at 70 h post-injection (3.3-fold, $P<0.0001$) (Fig. 2f, g). Overall, the ex vivo studies showed that OX26₅-F(ab')₂-Bapi was a more favourable PET ligand candidate.

[¹²⁴I]-OX26₅-F(ab')₂-Bapi PET visualized A β pathology in TgF344-AD rats and correlated with ex vivo brain distribution of [¹²⁴I]-OX26₅-F(ab')₂-Bapi

PET scans of TgF344-AD rats showed increased signal in the brain compared with baseline signals in the brains of WT rats, specifically in the cortex and cerebellum (Fig. 3a). Quantification of PET confirmed that TgF344-AD rats had 2- to 4-fold higher radioligand retention than WT rats, depending on the brain region ($P<0.01$, Fig. 3b). Furthermore, ex vivo analysis on perfused brains showed significantly higher [¹²⁴I]-OX26₅-F(ab')₂-Bapi retention in all brain regions in TgF344-AD rats compared with WT rats (18- to 32-fold, $P<0.01$, Fig. 3c). The PET signal quantification significantly correlated with ex vivo [¹²⁴I]-OX26₅-F(ab')₂-Bapi concentrations in TgF344-AD rat brains ($r^2=0.810$, $P<0.0001$, Fig. 3d). The brain-to-blood ratio was also significantly higher in TgF344-AD rats than WT rats ($P=0.0003$, Fig. 3e). The peripheral distribution of [¹²⁴I]-OX26₅-F(ab')₂-Bapi

was similar between TgF344-AD and WT rats (Fig. 3f), except that the WT animals had higher radioactivity concentrations in the spleen (1.2-fold, $P=0.0095$) and urine (2.1-fold, $P<0.0001$) compared with TgF344-AD rats. Finally, the blood pharmacokinetic profile was not affected by genotype. The TgF344-AD and WT rats had similar [¹²⁴I]-OX26₅-F(ab')₂-Bapi elimination curves in whole blood over 72 h post-administration (Additional file 1: Fig. S2a) and the percent in plasma at 72 h post-administration did not differ significantly ($P=0.76$, Additional file 1: Fig. S2b).

[¹²⁴I]-OX26₅-F(ab')₂-Bapi PET correlated with A β pathology

Ex vivo autoradiography performed on perfused brain sections showed increased signals in the cortex and cerebellum of TgF344-AD rats (Fig. 4). Sagittal sections stained for A β ₄₂ illustrated that TgF344-AD rats had abundant A β ₄₂ pathology in the cortex, caudate putamen, hippocampus and cerebellum, displaying both dense and diffuse A β deposits (Fig. 4). On the contrary, there was no A β ₄₂ pathology in WT rat brains.

ELISA analysis of brain homogenates revealed that A β levels did not differ significantly among cortex, hippocampus and cerebellum in TgF344-AD rats for total A β ₄₀, total A β ₄₂ or soluble A β aggregates (Fig. 5a). The PET signal quantification correlated with concentrations of total A β ₄₀ ($P<0.05$) and A β ₄₂ ($P<0.001$) but not with soluble A β aggregates (Fig. 5b).

Discussion

To investigate the role TfR affinity plays in transport of bispecific immunoPET ligands across the BBB, two bispecific fusion protein variants were produced. In vivo pharmacokinetic studies indicated that 72 h was a good time point for PET imaging since there was little immunoPET ligand signal left in the brains or blood of WT

(See figure on next page.)

Fig. 2 Ex vivo biodistribution of [¹²⁵I]-OX26₅-F(ab')₂-Bapi or [¹²⁴I]-OX26₇₆-F(ab')₂-Bapi in WT rats. **a** Concentration (SUV) of [¹²⁵I]-OX26₅-F(ab')₂-Bapi or [¹²⁴I]-OX26₇₆-F(ab')₂-Bapi in WT rat brain regions 4 h and 70 h post-administration. **b** Bispecific fusion protein distribution in brain capillaries and parenchyma 4 h post-administration. **c** Whole blood elimination curves over 3 days post-administration. Curve fit based on a two-phase decay non-linear regression model. **d, e** Brain-to-blood ratio (**d**) and percent in plasma (**e**) 4 h and 70 h post-administration. **f, g** Peripheral ex vivo biodistribution (SUV) of [¹²⁵I]-OX26₅-F(ab')₂-Bapi or [¹²⁴I]-OX26₇₆-F(ab')₂-Bapi in WT rats 4 h (**f**) and 70 h (**g**) post-administration. * $P\leq 0.05$, ** $P\leq 0.01$, *** $P\leq 0.001$, **** $P\leq 0.0001$

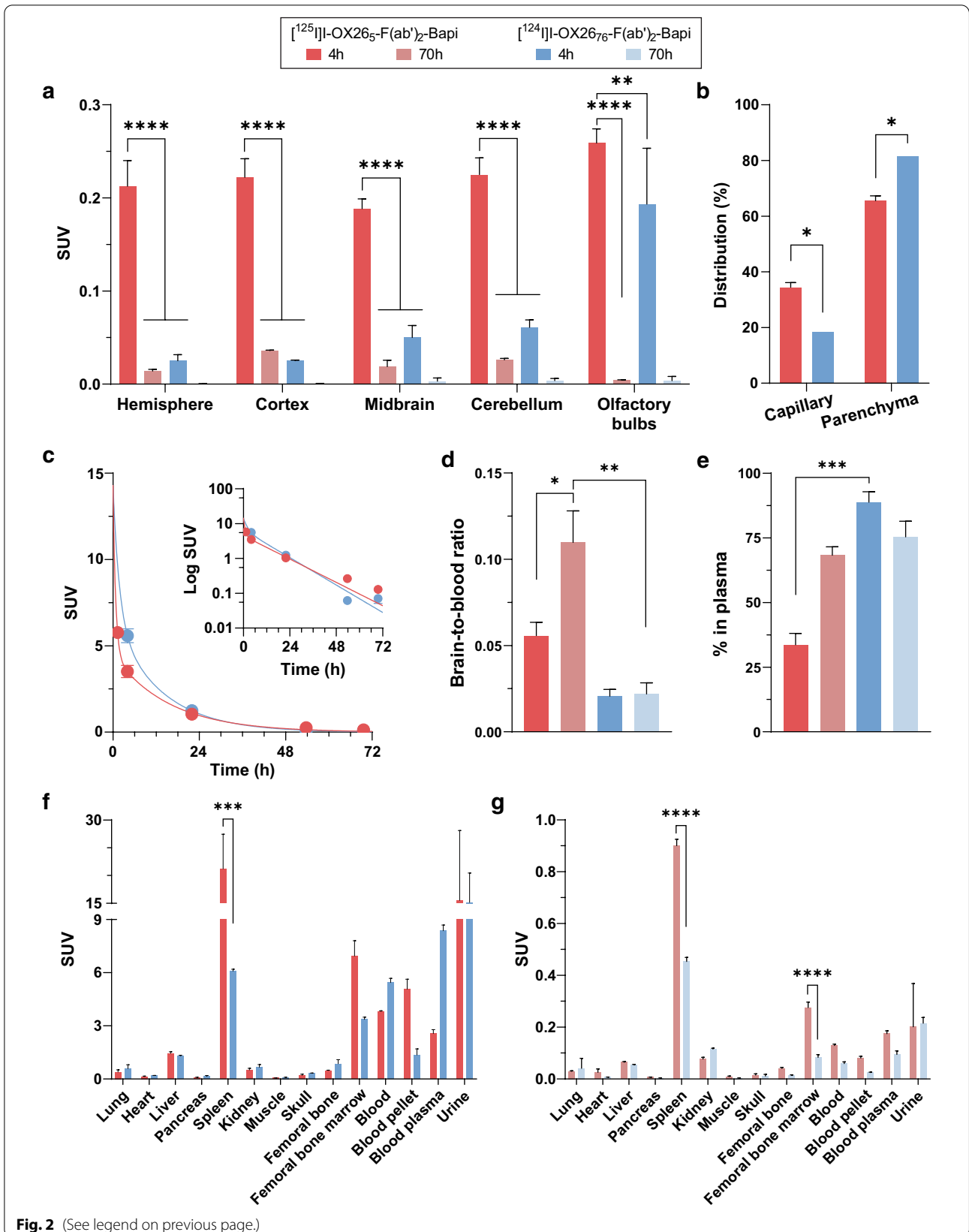


Fig. 2 (See legend on previous page.)

Table 4 Whole blood half-lives and area under the curve (AUC) for bispecific fusion protein variants

Variant	Half-life (h)		AUC
	Fast phase	Slow phase	
[¹²⁵ I]-OX26 ₅ -F(ab') ₂ -Bapi	0.50 (0.41–0.59)	10.78 (8.02–14.15)	77.34 (69.85–84.84)
[¹²⁴ I]-OX26 ₇₆ -F(ab') ₂ -Bapi	1.22 (0–2.41)	9.17 (7.13–25.96)	82.85 (73.09–92.62)

Data presented as mean (95% confidence intervals)

rats, suggesting good contrast for PET imaging. This time corresponded with immunoPET imaging of A β in two different transgenic AD mouse models [7, 28]. Furthermore, we found that at 4 h post-administration, there was significantly more [¹²⁵I]-OX26₅-F(ab')₂-Bapi in all brain areas compared with [¹²⁴I]-OX26₇₆-F(ab')₂-Bapi. These results contradict previous findings that the OX26₇₆ IgG enters the brain significantly better than the OX26₅ IgG [22, 36]. One explanation for the higher BBB transcytosis of [¹²⁵I]-OX26₅-F(ab')₂-Bapi is that the conjugation reaction may have an effect on the affinity of the parent antibody to rTfR. After conjugation, OX26₅-F(ab')₂-Bapi retained a similar rTfR affinity as the parental OX26₅ IgG. Unexpectedly, the in vitro affinity of OX26₇₆ to rTfR substantially decreased after conjugation, which likely led to the lower brain uptake of [¹²⁴I]-OX26₇₆-F(ab')₂-Bapi due to the poor interaction with endogenous TfR [18, 22, 35, 36]. This hypothesis is supported by the higher percent in plasma at 4 h, the longer half-life in the fast distribution phase in whole blood and the lower concentration in the spleen compared with [¹²⁵I]-OX26₅-F(ab')₂-Bapi, all of which indicate insufficient binding to TfR in vivo.

Dosage has also been suggested to influence the effect of TfR affinity on BBB transcytosis, such that higher-affinity binders enter the brain better at tracer doses [9, 16]. This dose-dependency hypothesis could explain the better brain uptake of [¹²⁵I]-OX26₅-F(ab')₂-Bapi since the max dose used here was 0.12 mg/kg, while previous reports with these OX26 variants used therapeutic doses of 10–20 mg/kg [22, 36]. Further studies are necessary to determine the extent to which dosing influences the effects of affinity, specifically for bispecific immunoPET radioligands.

ImmunoPET ligands with TfR-mediated brain uptake have proven more sensitive in detecting A β pathology than small-molecule tracers in mice [7, 28, 31, 32]. Previous PET analyses of the TgF344-AD rat model with the amyloid ligands [¹⁸F]FDDNP in 15-month-old rats and [¹⁸F]Florbetaben in 18-month-old rats both measured small differences in brain pathology between AD and WT rats (1.07- and 1.25-fold increases in signal, respectively) [41, 42]. ImmunoPET with [¹²⁴I]-OX26₅-F(ab')₂-Bapi in slightly younger TgF344-AD rats (14-month-old) showed 2- to 4-fold higher signals than WT littermates,

depending on brain region. Taken together, the data presented here indicate that immunoPET ligands may be more sensitive than small-molecule tracers in rats as well.

In TgF344-AD animals, the brain-region SUVs also correlated with the ex vivo levels of [¹²⁴I]-OX26₅-F(ab')₂-Bapi and with the total A β ₄₀ and A β ₄₂ levels detected by ELISA. Furthermore, the increased cortical and cerebellar PET signal corresponded with increased ex vivo autoradiography signal and abundant A β ₄₂ staining in these brain regions in TgF344-AD rats. These results suggest that the PET signal originated from radiolabelled bispecific fusion protein specifically binding to and around A β deposits in TgF344-AD rat brains. The high cortical, hippocampal and dorsal striatal (caudate and putamen) signals seen in the immunoPET scans, autoradiography and A β ₄₂ immunofluorescence correspond with descriptions of pathology in literature [41–43]. Cerebellar pathology has been reported to develop later than cortical and hippocampal pathology in TgF344-AD rats [41, 43]. Here, we noticed a strong PET signal in the cerebellum, which corresponds with the high concentration of A β in the brain tissue. One explanation for this strong cerebellar PET signal in comparison to previous PET studies [42] could be that, due to the overexpression of A β ₄₂ in this model and later development of cerebellar pathology, the cerebellum may contain proportionally more diffuse A β plaques than other brain regions. Diffuse deposits represent an earlier form of A β plaques [48] that are readily detected with [¹²⁴I]-OX26₅-F(ab')₂-Bapi but lack the amyloid core that is detected by traditional A β tracers.

Another difference from previous findings [28, 30, 32] is that in this study the PET signals did not correlate with the levels of soluble A β aggregates within AD animal groups. Furthermore, the correlations with total A β ₄₀ and A β ₄₂ were driven by one AD rat that had higher pathology than the others. This ligand clearly differentiated between AD and WT rats but the lack of strong correlations to A β pathology may be because the animals were at the same disease stage. In future studies, the ability of this radioligand to detect pathology changes at different ages and after therapeutic interventions should be explored.

One limitation in this study was the production of bispecific fusion proteins with chemical conjugation.

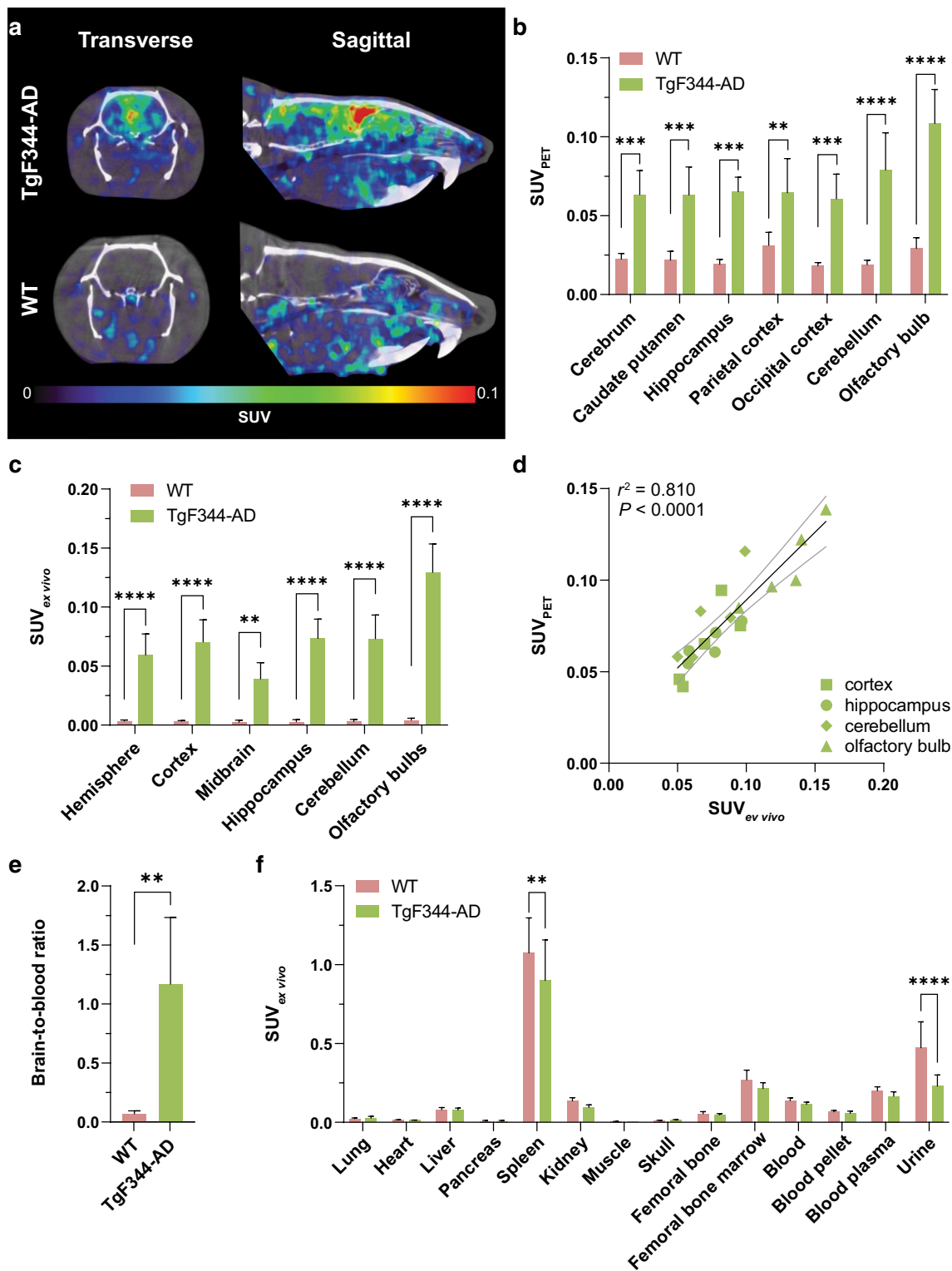


Fig. 3 [¹²⁴I]-OX26₅-F(ab')₂-Bapi PET images and quantification. **a** Representative in vivo PET images from TgF344-AD and WT rats 3 days post-administration of [¹²⁴I]-OX26₅-F(ab')₂-Bapi. **b** PET image-based quantification of [¹²⁴I]-OX26₅-F(ab')₂-Bapi distribution (SUV) in WT and TgF344-AD rat brains. **c** Ex vivo [¹²⁴I]-OX26₅-F(ab')₂-Bapi retention (SUV) in WT and TgF344-AD rat brains. **d** Pearson's correlation between PET-based quantification (SUV_{PET}) and ex vivo retention (SUV_{ex vivo}) of [¹²⁴I]-OX26₅-F(ab')₂-Bapi in four brain regions from TgF344-AD rats. **e** Brain-to-blood ratio in TgF344-AD and WT rats. **f** Peripheral ex vivo biodistribution (SUV) of [¹²⁴I]-OX26₅-F(ab')₂-Bapi in TgF344-AD and WT rats 3 days post-administration. ** $P \leq 0.01$, *** $P \leq 0.001$, **** $P \leq 0.0001$

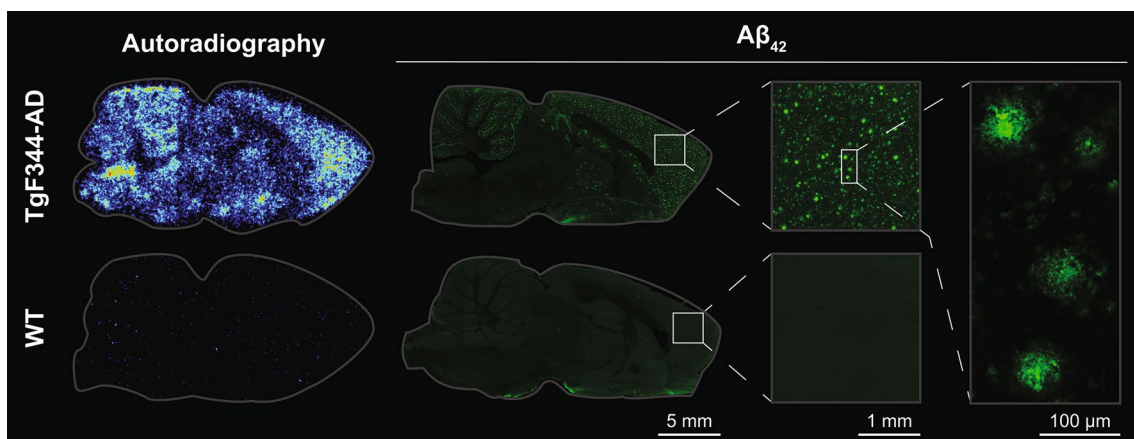


Fig. 4 Representative sagittal images of ex vivo autoradiography and Aβ₄₂ immunofluorescence from TgF344-AD and WT rats after [¹²⁴I] I-OX26₅-F(ab')₂-Bapi PET

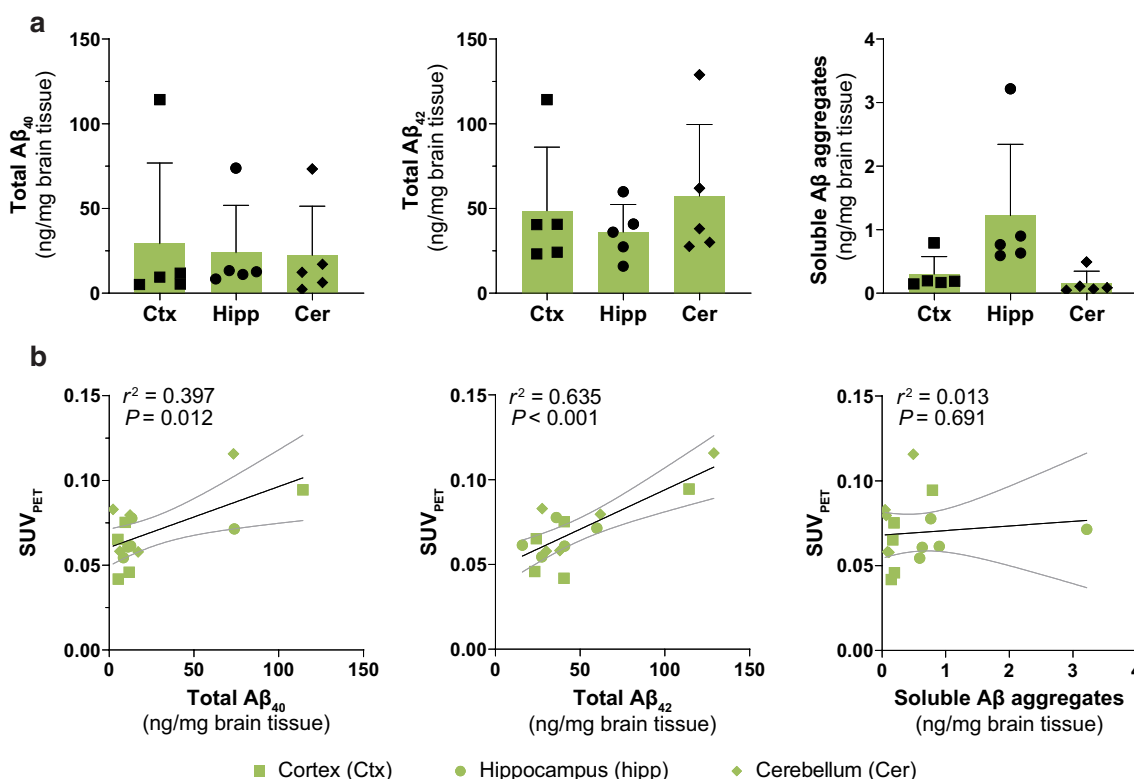


Fig. 5 **a** ELISA quantification of total Aβ₄₀, total Aβ₄₂ and soluble Aβ aggregates in brain regions from TgF344-AD rats. **b** Pearson's correlation between PET-based quantification (SUV_{PET}) and Aβ concentrations

The IEDDA reaction resulted in a heterogeneous product with OX26 IgG conjugated to 1–3 F(ab')₂-Bapi fragments. Further, the two moieties (OX26 IgG and F(ab')₂-Bapi) were conjugated randomly at different sites. This method is unsuitable to produce a clinically

applicable bispecific immunoPET radioligand. An alternative would be to use a site-specific conjugation method, such as Sortase A catalysed chemo-enzymatic reaction [49].

Conclusion

In conclusion, we have shown that Tfr affinity influences the BBB passage of bispecific immunoPET ligands. However, it remains unclear whether the dose of the bispecific antibody influences the effect of affinity. Finally, we have demonstrated that the Tfr-mediated transport of an immunoPET radioligand enables sensitive imaging of brain A β pathology in a rat model of AD, expanding its use over mice. Therefore, this strategy for delivery of immunoPET ligands to the CNS could eventually be translated from bench to bedside given the development of suitable human-specific Tfr-binders.

Abbreviations

[¹¹C]PIB: [¹¹C]Pittsburgh Compound B; A β : Amyloid-beta; AD: Alzheimer's disease; AUC: Area under the curve; Bapi: Bapineuzumab; BBB: Blood-brain barrier; BSA: Bovine serum albumin; CNS: Central nervous system; CT: Computed tomography; FA: Formic acid; HAC: Acetic acid; HRP: Horseradish peroxidase; IEDDA: Inverse electron demand Diels-Alder; MRI: Magnetic resonance image; OD: Optical density; PET: Positron emission tomography; PK: Pharmacokinetic; RT: Room temperature; rTfr: Rat transferrin receptor; SUV: Standardized uptake value; TCO: Trans-cyclooctene; TFR: Transferrin receptor.

Supplementary Information

The online version contains supplementary material available at <https://doi.org/10.1186/s40035-022-00324-y>.

Additional file 1. Fig S1. Representative sagittal images of A β pathology visualized with RmAb3D6, the murine version of Bapi, in 15-month-old TgF344-AD and WT rats. **Fig S2.** Ex vivo blood pharmacokinetics of [¹²⁴I]-I-OX26₅-F(ab')₂-Bapi in TgF344-AD and WT rats

Acknowledgements

We thank Rebecca Faresjö and Martin Larhammar for experimental support. The molecular imaging work in this study was performed at the SciLifeLab Pilot Facility for Preclinical PET-MRI, a Swedish nationally available imaging platform at Uppsala University, Sweden, financed by the Knut and Alice Wallenberg Foundation.

Author contributions

GB, DS, KGA and SS contributed to the study conception and design. MHS and FLP provided the TgF344 AD and WT littermate rats. GB performed material preparation. GB, DS and SS performed data collection. GB performed data analysis and wrote the first draft of the manuscript. All authors commented on previous versions of the manuscript and have read and approved the final manuscript.

Funding

Open access funding provided by Uppsala University. This project received funding from the European Union's Horizon 2020 research and innovation programme under the Marie Skłodowska-Curie Grant Agreement No. 813528, the Swedish Research Council (2017-02413, 2018-02715, 2021-1083 and 2021-03524), the Swedish Innovation Agency (2019-00106), Alzheimerfonden, Hjärnfonden, Hedlunds stiftelse, Torsten Söderbergs stiftelse, Åhlenstiftelsen, Stiftelsen för gamla tjänarinnor, Stohnes stiftelse, Magnus Bergvalls stiftelse, Konug Gustaf Vs och Drottning Victorias frimurarestiftelse, Åke Wibergs stiftelse and Turku University Hospital. The funding organizations did not take part in designing the study, in collecting, analysing, or interpreting the data, or in writing the manuscript.

Availability of data and materials

The datasets generated and/or analysed during the current study are available from the corresponding author on reasonable request.

Declarations

Ethics approval and consent to participate

All animal experiments described in this study were approved by the Uppsala County Animal Ethics board (5.8.18–20401/2020), following the rules and regulations of the Swedish Animal Welfare Agency and complied with the European Communities Council Directive of 22 September 2010 (2010/63/EU).

Consent for publication

Not applicable.

Competing interests

GB and KGA are employees of BioArctic AB, Sweden. The other authors declare that they have no competing interests.

Author details

¹Department of Public Health and Caring Sciences, Uppsala University, 751 85 Uppsala, Sweden. ²BioArctic AB, 112 51 Stockholm, Sweden. ³Preclinical Imaging Laboratory, Turku PET Centre, University of Turku, 20520 Turku, Finland. ⁴MediCity Research Laboratory, University of Turku, 20520 Turku, Finland.

Received: 12 July 2022 Accepted: 3 November 2022

Published online: 26 December 2022

References

- Ossenkoppelle R, Jansen WJ, Rabinovici GD, Knol DL, van der Flier WM, van Berckel BNM, et al. Prevalence of amyloid PET positivity in dementia syndromes: a meta-analysis. *JAMA*. 2015;313(19):1939–49.
- Lambert MP, Barlow AK, Chromy BA, Edwards C, Freed R, Liosatos M, et al. Diffusible, nonfibrillar ligands derived from A β 1–42 are potent central nervous system neurotoxins. *Proc Natl Acad Sci U S A*. 1998;95:6448–53.
- McLean CA, Cherny RA, Fraser FW, Fuller SJ, Smith MJ, Beyreuther K, et al. Soluble pool of A β amyloid as a determinant of severity of neurodegeneration in Alzheimer's disease. *Ann Neurol*. 1999;46(6):860–6.
- Schöll M, Wall A, Thordardottir S, Ferreira D, Bogdanovic N, Långström B, et al. Low PiB PET retention in presence of pathologic CSF biomarkers in Arctic APP mutation carriers. *Neurology*. 2012;79(3):229–36.
- Sehlin D, Syvänen S. Engineered antibodies: new possibilities for brain PET? *Eur J Nucl Med Mol Imaging*. 2019;11.
- Wei W, Rosenkrans ZT, Liu J, Huang G, Luo QY, Cai W. ImmunoPET: concept, design, and applications. *Chem Rev*. 2020;120(8):3787–851.
- Meier SR, Sehlin D, Roshanbin S, Lim Falk V, Saito T, Saido TC, et al. 11 C-PiB and ¹²⁴I-antibody PET provide differing estimates of brain amyloid-beta after therapeutic intervention. *J Nucl Med*. 2022;63(2):302–9.
- Magnusson K, Sehlin D, Syvänen S, Svedberg MM, Philipson O, Söderberg L, et al. Specific uptake of an amyloid- β protofibril-binding antibody-tracer in A β PP transgenic mouse brain. *J Alzheimers Dis*. 2013;37(1):29–40.
- Hultqvist G, Syvänen S, Fang XT, Lannfelt L, Sehlin D. Bivalent brain shuttle increases antibody uptake by monovalent binding to the transferrin receptor. *Theranostics*. 2017;7(2):308–18.
- Syvänen S, Hultqvist G, Gustavsson T, Gumucio A, Laudon H, Söderberg L, et al. Efficient clearance of A β protofibrils in A β PP-transgenic mice treated with a brain-penetrating bifunctional antibody. *Alzheimers Res Ther*. 2018;10(1):1–10.
- Sehlin D, Stocki P, Gustavsson T, Hultqvist G, Walsh FS, Rutkowski JL, et al. Brain delivery of biologics using a cross-species reactive transferrin receptor 1 VNAR shuttle. *FASEB J*. 2020;34(10):13272–83.
- Stanimirovic DB, Sandhu JK, Costain WJ. Emerging technologies for delivery of biotherapeutics and gene therapy across the blood-brain barrier. *BioDrugs*. 2018;32(6):547–59.
- Johnsen KB, Burkhart A, Thomsen LB, Andresen TL, Moos T. Targeting the transferrin receptor for brain drug delivery. *Prog Neurobiol*. 2019;181:101665.
- Zhao Z, Zlokovic BV. Therapeutic TVs for crossing barriers in the brain. *Cell*. 2020;182(2):267–9.

15. Boado RJ, Zhou QH, Lu JZ, Hui EKW, Pardridge WM. Pharmacokinetics and brain uptake of a genetically engineered bifunctional fusion antibody targeting the mouse transferrin receptor. *Mol Pharm.* 2010;7(1):237–44.
16. Yu YJ, Zhang Y, Kenrick M, Hoyte K, Luk W, Lu Y, et al. Boosting brain uptake of a therapeutic antibody by reducing its affinity for a transcytosis target. *Sci Transl Med.* 2011;3(84):1–9.
17. Niewoehner J, Bohrmann B, Collin L, Ulrich E, Sade H, Maier P, et al. Increased brain penetration and potency of a therapeutic antibody using a monovalent molecular shuttle. *Neuron.* 2014;81(1):49–60.
18. Webster CI, Hatcher J, Burrell M, Thom G, Thornton P, Gurrell I, et al. Enhanced delivery of IL-1 receptor antagonist to the central nervous system as a novel anti-Transferrin receptor-IL-1RA fusion reverses neuro-pathic mechanical hypersensitivity. *Pain.* 2017;158(4):660–8.
19. Rofo F, Yilmaz CU, Metzendorf N, Gustavsson T, Beretta C, Erlandsson A, et al. Enhanced neprilysin-mediated degradation of hippocampal A β 42 with a somatostatin peptide that enters the brain. *Theranostics.* 2020;11(2):789–804.
20. Friden PM, Walus LR, Musso GF, Taylor MA, Malfroy B, Starzyk RM. Anti-transferrin receptor antibody and antibody-drug conjugates cross the blood-brain barrier. *Proc Natl Acad Sci U S A.* 1991;88(11):4771–5.
21. Wu D, Pardridge WM. Neuroprotection with noninvasive neurotrophin delivery to the brain. *Proc Natl Acad Sci U S A.* 1999;96(1):254–9.
22. Thom G, Burrell M, Haqqani AS, Yogi A, Lessard E, Brunette E, et al. Enhanced delivery of galanin conjugates to the brain through bioengineering of the anti-transferrin receptor antibody OX26. *Mol Pharm.* 2018;15(4):1420–31.
23. Campos CR, Kemble AM, Niewoehner J, Freskgård PO, Ulrich E. Brain shuttle neprilysin reduces central amyloid- β levels. *PLoS One.* 2020;15(3):1–12.
24. Yu YJ, Atwal JK, Zhang Y, Tong RK, Wildsmith KR, Tan C, et al. Therapeutic bispecific antibodies cross the blood-brain barrier in nonhuman primates. *Sci Transl Med.* 2014;6(261):1–11.
25. Sonoda H, Morimoto H, Yoden E, Koshimura Y, Kinoshita M, Golovina G, et al. A blood-brain-barrier-penetrating anti-human transferrin receptor antibody fusion protein for neuronopathic mucopolysaccharidosis II. *Mol Ther.* 2018;26(5):1366–74.
26. Kariolis MS, Wells RC, Getz JA, Kwan W, Mahon CS, Tong R, et al. Brain delivery of therapeutic proteins using an Fc fragment blood-brain barrier transport vehicle in mice and monkeys. *Sci Transl Med.* 2020;12(545):1–14.
27. Terstappen GC, Meyer AH, Bell RD, Zhang W. Strategies for delivering therapeutics across the blood-brain barrier. *Nat Rev Drug Discov.* 2021;20(5):362–83.
28. Sehlin D, Fang XT, Cato L, Antoni G, Lannfelt L, Syvänen S. Antibody-based PET imaging of amyloid beta in mouse models of Alzheimer's disease. *Nat Commun.* 2016;7:1–11.
29. Sehlin D, Fang XT, Meier SR, Jansson M, Syvänen S. Pharmacokinetics, biodistribution and brain retention of a bispecific antibody-based PET radioligand for imaging of amyloid- β . *Sci Rep.* 2017;7(1):1–9.
30. Syvänen S, Fang XT, Hultqvist G, Meier SR, Lannfelt L, Sehlin D. A bispecific Tribody PET radioligand for visualization of amyloid-beta protofibrils—a new concept for neuroimaging. *NeuroImage.* 2017;148:55–63.
31. Meier SR, Syvänen S, Hultqvist G, Fang XT, Roshanbin S, Lannfelt L, et al. Antibody-based in vivo PET imaging detects amyloid- β reduction in Alzheimer transgenic mice after BACE-1 inhibition. *J Nucl Med.* 2018;59(12):1901–6.
32. Fang XT, Hultqvist G, Meier SR, Antoni G, Sehlin D, Syvänen S. High detection sensitivity with antibody-based PET radioligand for amyloid beta in brain. *NeuroImage.* 2019;184(October):881–8.
33. Syvänen S, Fang XT, Faresjö R, Rokka J, Lannfelt L, Olberg DE, et al. Fluorine-18-labeled antibody ligands for PET imaging of amyloid- β in brain. *ACS Chem Neurosci.* 2020;11(24):4460–8.
34. Bien-Ly N, Yu YJ, Bumbaca D, Elstrott J, Boswell CA, Zhang Y, et al. Transferrin receptor (TfR) trafficking determines brain uptake of TfR antibody affinity variants. *J Exp Med.* 2014;211(2):233–44.
35. Haqqani AS, Thom G, Burrell M, Delaney CE, Brunette E, Baumann E, et al. Intracellular sorting and transcytosis of the rat transferrin receptor antibody OX26 across the blood-brain barrier in vitro is dependent on its binding affinity. *J Neurochem.* 2018;146(6):735–52.
36. Chang HY, Wu S, Li Y, Zhang W, Burrell M, Webster CI, et al. Brain pharmacokinetics of anti-transferrin receptor antibody affinity variants in rats determined using microdialysis. *MAbs.* 2021;13(1).
37. Faresjö R, Bonvicini G, Fang XT, Aguilar X, Sehlin D, Syvänen S. Brain pharmacokinetics of two BBB penetrating bispecific antibodies of different size. *Fluids Barriers CNS.* 2021;18(1):1–15.
38. Jefferies WA, Brandon MR, Hunt SV, Williams AF, Gatter KC, Mason DY. Transferrin receptor on endothelium of brain capillaries. *Nature.* 1984;312(5990):162–3.
39. Abushouk AI, Elmaraezy A, Aglan A, Salama R, Fouda S, Fouda R, et al. Bapineuzumab for mild to moderate Alzheimer's disease: a meta-analysis of randomized controlled trials. *BMC Neurol.* 2017;17(1):1–13.
40. Greenwood FC, Hunter WM, Glover JS. The preparation of I-131-labelled human growth hormone of high specific. *Biochem J.* 1963;89:114–23.
41. Cohen RM, Rezai-Zadeh K, Weitz TM, Rentsendorj A, Gate D, Spivak I, et al. A transgenic Alzheimer rat with plaques, tau pathology, behavioral impairment, oligomeric A β , and frank neuronal loss. *J Neurosci.* 2013;33(15):6245–56.
42. Chaney AM, Lopez-Picon FR, Serrière S, Wang R, Bochicchio D, Webb SD, et al. Prodromal neuroinflammatory, cholinergic and metabolite dysfunction detected by PET and MRS in the TgF344-AD transgenic rat model of AD: A collaborative multi-modal study. *Theranostics.* 2021;11(14):6644–67.
43. Saré RM, Cooke SK, Krych L, Zerfas PM, Cohen RM, Smith CB. Behavioral phenotype in the TgF344-AD rat model of Alzheimer's disease. *Front Neurosci.* 2020;14:601.
44. Argent NB, Liles J, Rodham D, Clayton CB, Wilkinson R, Baylis PH. A new method for measuring the blood volume of the rat using ^{113m}Indium as a tracer. *Lab Anim.* 1994;28(2):172–5.
45. Loening AM, Gambhir SS. AMIDE: A free software tool for multimodality medical image analysis. *Mol Imaging.* 2003;2(3):131–7.
46. Buitter HJC, van Velden FHP, Leysen JE, Fisher A, Windhorst AD, Lam-mertsma AA, et al. Reproducible analysis of rat brain PET studies using an additional [¹⁸F]NaF scan and an MR-based ROI template. *Int J Mol Imaging.* 2012;2012:58071:1–10.
47. Gustafsson S, Gustavsson T, Roshanbin S, Hultqvist G, Hammarlund-Udenaes M, Sehlin D, et al. Blood-brain barrier integrity in a mouse model of Alzheimer's disease with or without acute 3D6 immunotherapy. *Neuropharm.* 2018;143:1–9.
48. Michno W, Nyström S, Wehrli P, Lashley T, Brinkmalm G, Guerard L, et al. Pyroglutamation of amyloid- β x-42 (A β x-42) followed by A β 1–40 deposition underlies plaque polymorphism in progressing Alzheimer's disease pathology. *J Biol Chem.* 2019;294(17):6719–32.
49. Tsukiji S, Nagamune T. Sortase-mediated ligation: a gift from gram-positive bacteria to protein engineering. *ChemBioChem.* 2009;10(5):787–98.

Ready to submit your research? Choose BMC and benefit from:

- fast, convenient online submission
- thorough peer review by experienced researchers in your field
- rapid publication on acceptance
- support for research data, including large and complex data types
- gold Open Access which fosters wider collaboration and increased citations
- maximum visibility for your research: over 100M website views per year

At BMC, research is always in progress.

Learn more biomedcentral.com/submissions

